Article

Current Biology

NIK/MAP3K14 Regulates Mitochondrial Dynamics and Trafficking to Promote Cell Invasion

Graphical Abstract

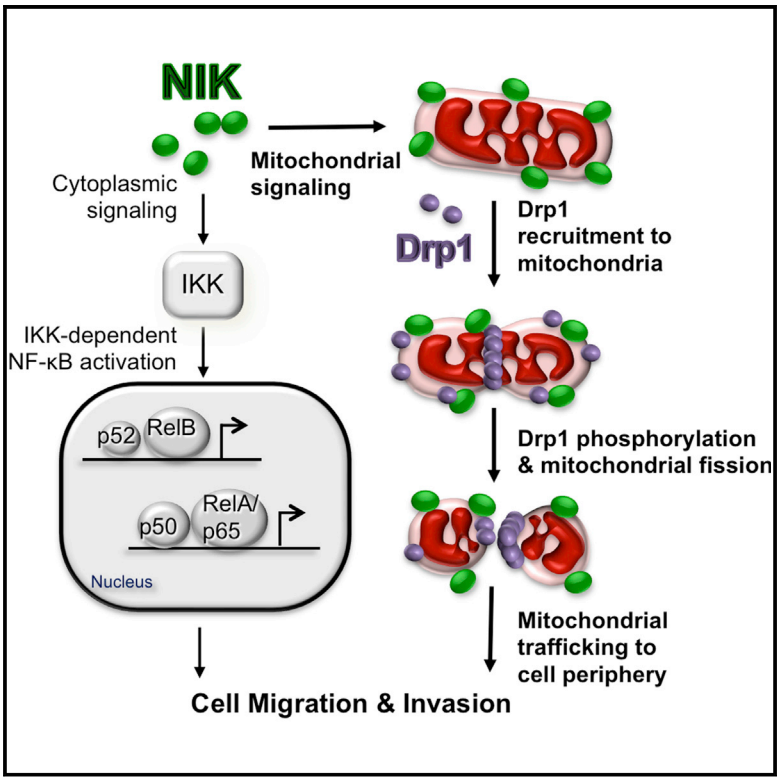

Highlights

- NIK localizes to mitochondria in MEFs, cancer cell lines, and ex vivo tumor tissue
- NIK regulates mitochondrial velocity and anterograde movement to the cell periphery
- NIK enhances fission, Drp1 phosphorylation, and Drp1 mitochondrial localization
- NIK regulates invasion and mitochondrial dynamics independent of IKK/NF-κB

Authors

Ji-Ung Jung, Sowndharya Ravi, Dong W. Lee, Kassandra McFadden, Michael L. Kamradt, L. Gerard Toussaint, Raquel Sitcheran

Correspondence

sitcheran@tamhsc.edu

In Brief

Jung et al. identify novel functions of NIK in regulating mitochondrial dynamics and tumor cell invasion through control of Drp1 phosphorylation and mitochondrial trafficking to the leading edge of migrating cells. These properties do not require NIK's downstream targets, IKKα/β, establishing a new paradigm for NIK signaling in mitochondria.

Jung et al., 2016, Current Biology *26*, 3288–3302
December 19, 2016
http://dx.doi.org/10.1016/j.cub.2016.10.009

CellPress

Current Biology
Article

NIK/MAP3K14 Regulates Mitochondrial Dynamics and Trafficking to Promote Cell Invasion

Ji-Ung Jung,[1,4] Sowndharya Ravi,[1,4] Dong W. Lee,[1] Kassandra McFadden,[1] Michael L. Kamradt,[1] L. Gerard Toussaint,[2,3] and Raquel Sitcheran[1,3,5,*]

[1]Department of Molecular and Cellular Medicine, Texas A&M Health Science Center, College Station, TX 77843-1114, USA
[2]Department of Neuroscience and Experimental Therapeutics, Texas A&M Health Science Center, College Station, TX 77807-3260, USA
[3]The Texas Brain and Spine Institute, Bryan, TX 77807, USA
[4]Co-first author
[5]Lead Contact
*Correspondence: sitcheran@tamhsc.edu
http://dx.doi.org/10.1016/j.cub.2016.10.009

SUMMARY

Although the role of NF-κB-inducing kinase (NIK) in immunity is well established, its relevance in cancer is just emerging. Here we describe novel functions for NIK in regulating mitochondrial dynamics and motility to promote cell invasion. We show that NIK is localized to mitochondria in cancer cell lines, ex vivo tumor tissue, and mouse embryonic fibroblasts (MEFs). NIK promotes mitochondrial fission, velocity, and directional migration, resulting in subcellular distribution of mitochondria to the periphery of migrating cells. Moreover, NIK is required for recruitment of Drp1 to mitochondria, forms a complex with Drp1, and regulates Drp1 phosphorylation at Ser-616 and dephosphorylation at Ser-637. Consistent with a role for NIK in regulating mitochondrial dynamics, we demonstrate that Drp1 is required for NIK-dependent, cytokine-induced invasion. Importantly, using MEFs, we demonstrate that the established downstream mediators of NIK signaling, IκB kinase α/β (IKKα/β) and NF-κB, are not required for NIK to regulate cell invasion, Drp1 mitochondrial localization, or mitochondrial fission. Our results establish a new paradigm for IKK-independent NIK signaling and significantly expand the current dogma that NIK is predominantly cytosolic and exclusively regulates NF-κB activity. Overall, these findings highlight the importance of NIK in tumor pathogenesis and invite new therapeutic strategies that attenuate mitochondrial dysfunction through inhibition of NIK and Drp1.

INTRODUCTION

NF-κB-inducing kinase (NIK; also known as MAP3K14), the central activator of the noncanonical NF-κB pathway, has been shown to promote tumorigenesis through its ability to regulate cell proliferation and survival [1, 2]. However, the molecular mechanisms by which NIK stimulates tumor growth have not been fully elucidated. Our previous work demonstrated that noncanonical NF-κB signaling is significantly increased in highly invasive glioma tumor lines compared to less invasive glioma lines [3, 4]. More recently, we have shown that the ability of NIK to promote glioma invasiveness is associated with the formation of extensive cell-membrane protrusions, termed pseudopodia or invadopodia [5], a subcellular region requiring high energy due to extensive cytoskeletal and focal adhesion remodeling during cell movement [6]. Consistent with a need to meet the energy demands of invasion, mitochondria have been observed to move to invadopodia at the leading edge of cancer cells [7, 8]. Moreover, tumor cell migration and invasion have been linked to regulation of mitochondrial dynamics, and more specifically to alterations in the balance between mitochondrial fission and fusion [9–11]. Indeed, cancer cells often exhibit a fragmented mitochondrial phenotype [12]. Consistent with these observations, the mitochondria-associated fission protein dynamin-related protein 1 (Drp1) has been shown to promote tumor migration and pathogenesis [10, 13].

Regulation of NIK, a constitutively active kinase [14], occurs primarily at the post-translational level. In unstimulated cells, NIK is rendered inactive through its association with a translocon associated protein complex (TRAF)-cellular inhibitor of apoptosis (cIAP) complex that catalyzes its ubiquitination and continuous proteasome-dependent degradation in the cytosol [15]. Activation of NIK is achieved through disassembly of the degradation complex, resulting in stabilization and accumulation of NIK protein [16]. Once stabilized, NIK phosphorylates and activates IKKα, which in turn phosphorylates p100, triggering proteolytic processing to p52 and nuclear translocation of p52-RelB noncanonical NF-κB transcription factors [16, 17]. The predominant, physiological function of NIK is to activate IKKα and noncanonical NF-κB signaling, but NIK can also induce IKKβ-dependent, canonical NF-κB signaling, particularly when NIK is overexpressed or aberrantly stabilized [18–20]. Here we describe novel roles for NIK in regulating mitochondrial dynamics to promote tumor cell invasion.

RESULTS

NIK Alters Mitochondrial Subcellular Distribution and Is Localized to Mitochondria in Cancer Cells

Proteomics analysis has revealed an enrichment of mitochondrial proteins in invadopodia [21], and recent cell-biological

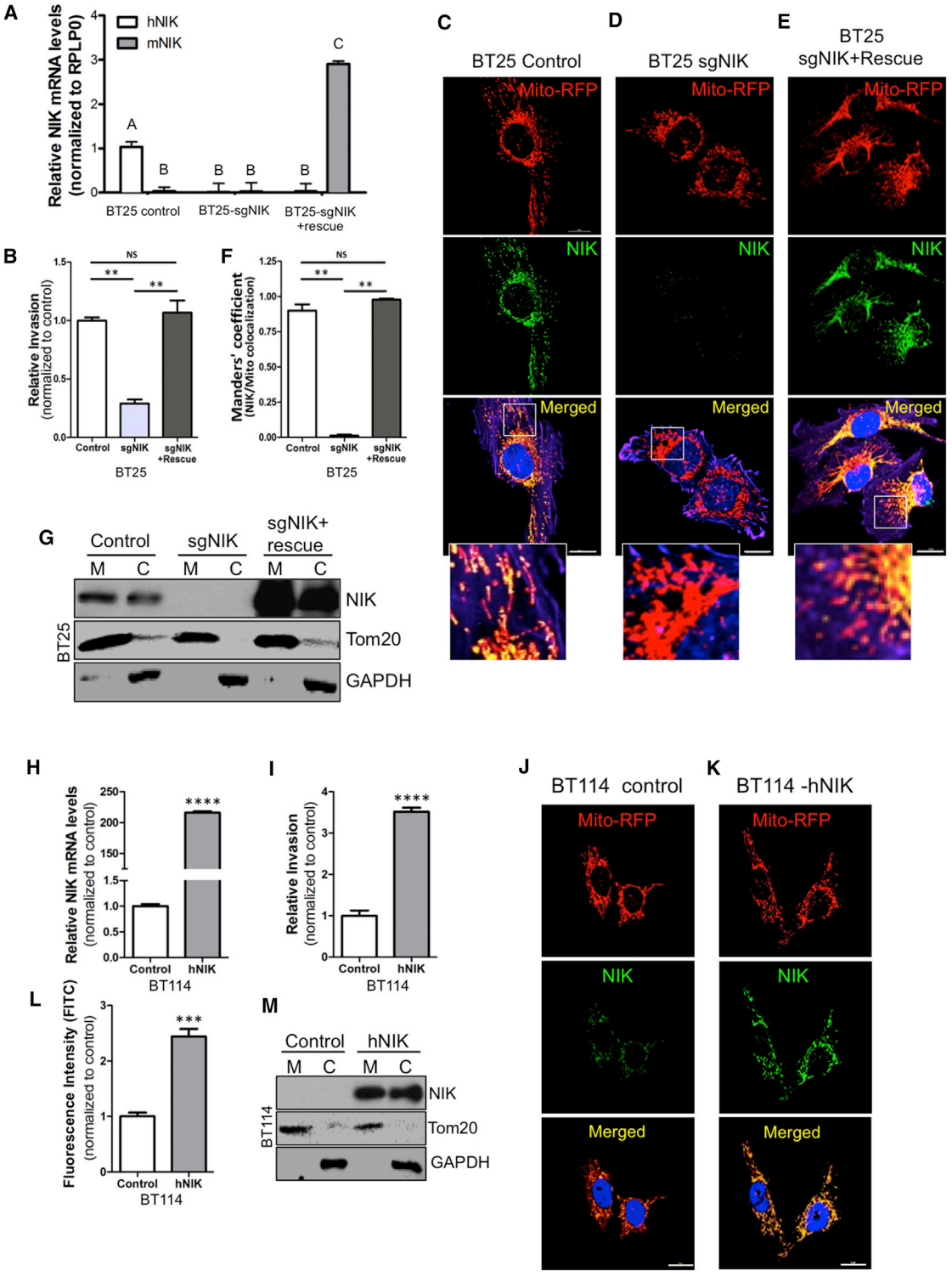

Figure 1. NIK Alters Mitochondrial Subcellular Distribution and Is Localized to Mitochondria in Cancer Cells

(A) qRT-PCR analysis of human and mouse NIK expression in human glioma cells: BT25 control, BT25-sgNIK, and BT25-sgNIK cells expressing mouse NIK (sgNIK+rescue). For this and all subsequent experiments, representative data from at least three independent experiments are shown. The graph shows mean values ± SD (n = 3). Different letters indicate statistically significant differences: for A versus B, $p < 0.001$; for A/B versus C, $p < 0.0001$.

(B) NIK expression correlates with invasive potential in 3D collagen invasion assays. Relative invasion reflects the numbers of invading cells normalized to control, and data are represented as mean ± SD. **$p < 0.001$ for sgNIK versus control and sgNIK versus sgNIK+rescue, one-way ANOVA.

(legend continued on next page)

studies have shown a re-distribution of mitochondria to the leading edge of cells during migration [7, 8]. These observations suggest that mitochondria move to distal cell protrusions and sites of active cell invasion. In light of our recent findings that NIK promotes invasion of glioma cells and induces cell-shape changes, including pseudopodia/invadopodia formation [5], we sought to determine whether NIK plays a role in these processes using a highly invasive (BT25) and a minimally invasive (BT114) glioma cell line that express high and low levels of NIK, respectively (Figures S1A and S1B) [4]. We first investigated NIK's role in BT25 cells and employed small guide (sg)RNAs in combination with CRISPR-Cas9 genome editing to generate BT25 tumor cells lacking a functional *NIK* gene (BT25-sgNIK) [5]. Loss of NIK significantly attenuates invasion in 3D collagen matrices compared with control cells, and invasion was restored with expression of the highly conserved murine NIK (BT25-sgNIK+rescue) (Figures 1A and 1B).

To visualize mitochondria, we transfected BT25 control, BT25-sgNIK, and BT25-sgNIK+rescue cells with the mitochondrial marker CellLight Mitochondria-RFP (Mito-RFP) [22]. Confocal fluorescence microscopy revealed that mitochondria extended throughout the cell body to sites distal from the nucleus (Figure 1C). However, Mito-RFP staining appeared collapsed around the nucleus of BT25-sgNIK cells, which had minimal cytoplasmic processes (Figure 1D), whereas BT25-sgNIK+rescue cells exhibited mitochondrial staining similar to control cells (Figure 1E). Interestingly, when we performed NIK immunostaining to confirm alterations in NIK expression, we observed a striking co-localization of NIK with Mito-RFP in untreated BT25 control cells (Figures 1C and 1F). Minimal NIK immunostaining was observed in BT25-sgNIK cells, demonstrating specificity of the antibody (Figure 1D), and re-expression of murine NIK (BT25-sgNIK+rescue cells) restored NIK mitochondrial staining (Figures 1E and 1F). For detection of endogenous NIK protein by immunoblotting, cells were treated with tumor necrosis factor-like weak inducer of apoptosis (TWEAK) (to induce NIK/noncanonical NF-κB signaling) [4] and the proteasome inhibitor MG132 (to stabilize NIK protein). NIK protein was present in both mitochondria-enriched (M) and cytosolic (C) cell fractions of TWEAK/MG132-treated BT25 control cells and BT25-sgNIK+rescue cells (Figure 1G). However, mitochondrial, but not cytosolic, NIK was readily detected by immunostaining (see Figures 1C and 1E), suggesting that antibody epitope availability differs in the cytosolic and mitochondrial compartments. NIK protein was not detected by immunoblotting in either fraction from BT25-sgNIK cells, confirming NIK knockout, as well as antibody specificity (Figure 1G).

We next confirmed NIK's function in mitochondria using gain-of-function studies in BT114 glioma cells. Interestingly, BT114 control cells displayed a mitochondrial phenotype that resembled BT25-sgNIK cells, with a concentration of perinuclear Mito-RFP signal (compare Figure 1J to Figure 1D). Overexpression of human NIK (BT114-hNIK) robustly increased invasion compared to BT114 control cells (Figures 1H and 1I). Furthermore, BT114-hNIK cells exhibited increased Mito-RFP staining throughout distal regions of the cell (Figures 1K and 1L). Although much weaker than BT25 cells, NIK immunostaining signal similarly co-localized with Mito-RFP in BT114 control cells (Figure 1J). We were unable to detect any NIK in untreated BT114 cells (without TWEAK/MG132) by immunoblotting (Figure 1M). However, ectopically expressed NIK protein was observed in both mitochondrial and cytosolic fractions of BT114-hNIK cells (Figure 1M).

Given the close association of mitochondria with other organelles, particularly the endoplasmic reticulum (ER), as well as a recent report describing localization of a small fraction of NIK to endosomes in endothelial cells [23], we examined NIK subcellular localization in more detail in BT25 glioma cells. Triple-immunostaining experiments showed that NIK expression overlapped extensively with mitochondrial cytochrome C oxidase subunit 4 (CoxIV), but not the ER protein calnexin (Figure 2A). Consistent with this observation, NIK showed extensive co-localization with the protein translocase of outer mitochrondrial membrane 20 (Tom20) but not the ER protein Sec61 (Figures 2B and 2C) or the endosomal Ras-related protein Rab-5 (Rab5) (Figure 2D).

To test whether mitochondrial localization of NIK, as well as its effect on mitochondrial intracellular distribution, was restricted to glioma cells, we performed immunostaining and invasion assays in MDA-MB231 breast cancer cells and Panc1

(C–E) Immunofluorescence images of BT25 control (C), BT25-sgNIK (D), and BT25-sgNIK+rescue cells (E) transfected with Mito-RFP (red) and immunostained for NIK (green) and DAPI (blue). Images marked with white squares are amplified and shown at the bottom. Scale bars, 10 μm.

(F) Bar graph showing Manders' coefficients (fraction of NIK in co-localization with Mito-RFP) for co-localization of NIK and mitochondria (C–E). Data are represented as mean ± SD (n = 12). **p < 0.01 for sgNIK versus control and sgNIK versus sgNIK+rescue, one-way ANOVA.

(G) Immunoblot analysis of mitochondria-enriched (M) and cytosolic (C) fractions prepared from BT25 control, BT25-sgNIK, and BT25-sgNIK+rescue cells pretreated with TWEAK (10 ng/mL) and MG132 (5 μM) to stabilize NIK for facile detection and to confirm the loss of protein in sgNIK cells. Four times the volume equivalent of mitochondria-enriched fraction versus cytosolic fraction was loaded (mitochondria-enriched/cytosol 4:1). Blots were probed with the indicated antibodies.

(H) qPCR analysis of NIK expression in BT114 control and BT114-hNIK cells. Data are represented as mean ± SD. ****p < 0.0001, unpaired t test.

(I) Quantification of 3D collagen invasion assays comparing BT114 control and BT114-hNIK cells. Data are represented as mean ± SEM. ****p < 0.001, unpaired t test.

(J and K) Representative confocal immunofluorescence images are shown of BT114 control (J) and BT114-hNIK cells (K) transfected with Mito-RFP and then immunostained for NIK (green) and DAPI (blue).

(L) Bar graph showing results from measurements of mean fluorescence intensity of NIK staining in BT114 control (J) and BT114-hNIK cells (K) normalized to control and represented as mean ± SEM (n = 30). ***p < 0.001, unpaired t test.

(M) Immunoblot analysis of cell fractions prepared from untreated BT114 control and BT114-hNIK cells using the indicated antibodies (mitochondria-enriched/cytosol 4:1 in volume equivalents).

See also Figure S1.

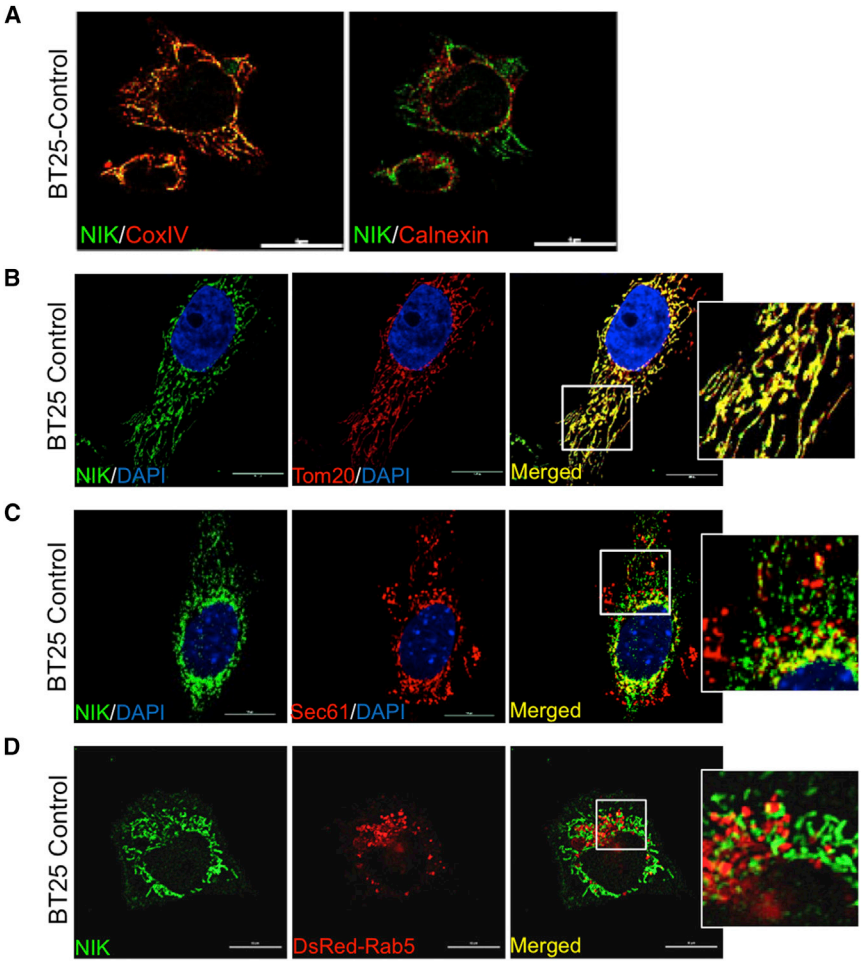

Figure 2. NIK Co-localization with Different Organelle Markers in Glioma Cells

(A) Representative confocal immunofluorescence images of BT25 cells sequentially triple-stained with antibodies specific for the mitochondrial marker CoxIV (AF564), endoplasmic reticulum marker calnexin (AF647), and polyclonal NIK (ab7204; Abcam). NIK-specific antibody was pre-labeled with AF488. Left: merged overlay (yellow-orange) of NIK (green) and CoxIV (red). Right: the same cell with a merged overlay of NIK (green) and calnexin (pseudo-colored red). Scale bars, 10 μm.

(B) Representative confocal immunofluorescence images of BT25 glioma cells immunostained for NIK (green) and a pre-labeled antibody specific for Tom20-AF647 (pseudo-colored red, upper panels). Images marked with white squares are amplified and shown on the right. Scale bars, 10 μm.

(C) Representative confocal immunofluorescence images of BT25 glioma cells immunostained for NIK (AF564; pseudo-colored green) and a pre-labeled antibody specific for Sec61A-AF488 (pseudo-colored red) and DAPI (blue). Images marked with white squares are amplified and shown on the right. Scale bars, 10 μm.

(D) Representative immunofluorescence confocal microscopy images of BT25 cells transfected with dsRed-Rab5 and then fixed and stained with an antibody specific to NIK (green). Images marked with white squares are amplified and shown on the right. Scale bars, 10 μm.

For (B)–(D), the NIK-specific antibody ab191591 (Abcam) was used. See also Figure S1 and Movies S1, S2, S3, S4, and S5.

pancreatic cancer cells. As with glioma cell lines, we observed co-localization of NIK and Mito-RFP in MDA-MB231 and Panc1 cells (Figures S1C and S1D, upper panels), and NIK immunostaining was lost in CRISPR-Cas9-mediated NIK knockout cells (Figures S1C and S1D, lower panels), similar to BT25 knockout cells. Moreover, loss of NIK in MDA-MB231-sgNIK and Panc1-sgNIK cells resulted in condensed, perinuclear Mito-RFP staining and significantly diminished invasive potential (Figures S1C–S1E). Together, these data identify a previously unknown pool of NIK protein that localizes to mitochondria in several different cancer cells and demonstrate a strong correlation between mitochondrial NIK expression and cell invasion.

NIK Regulates Mitochondrial Subcellular Localization, Motility, and Morphology

To analyze NIK's role in mitochondrial clustering in more detail, we quantified intracellular mitochondrial distribution in migrating BT25, BT25-sgNIK, and BT25-sgNIK+rescue cells. Fluorescence intensity plots demonstrated that mitochondria in BT25 control cells extended from the nucleus to the distal edge of cells (Figure 3A). Mitochondria in cells lacking NIK extended less than half the distance of those organelles in control cells, and remained collapsed in the perinuclear region (Figure 3A). As expected, NIK overexpression (BT25-sgNIK+rescue cells) restored the presence of mitochondria from the nucleus to the distal edge, similar to control cells (Figure 3A). To determine whether the accumulation of perinuclear mitochondria was associated with decreased mitochondrial motility during cell migration, we performed time-lapse imaging and particle-tracking analysis of Mito-RFP-labeled mitochondria. Results from these experiments revealed that the velocity and overall distance traveled by mitochondria was significantly compromised in BT25-sgNIK cells, and these defects were restored by re-expression of NIK (BT25-sgNIK+rescue cells; Figures 3B and 3C; Movies S1, S2, and S3). Moreover, mitochondria in BT25 control and BT25-sgNIK+rescue cells exhibited predominantly anterograde movement and directional migration toward the cell periphery, whereas mitochondria in BT25-sgNIK cells exhibited seemingly random patterns of both anterograde and retrograde movement (Figure 3D; Movies S1, S2, and S3).

We next performed superresolution-structured illumination microscopy of Mito-RFP-labeled BT25 cells. Results from these experiments demonstrated that mitochondria in BT25 control cells were fragmented, forming elongated tracks throughout the cytoplasm that extended toward the cell periphery (Figure 3E). In BT25-sgNIK cells, however, mitochondria were more tangled, fused, and condensed around the nucleus

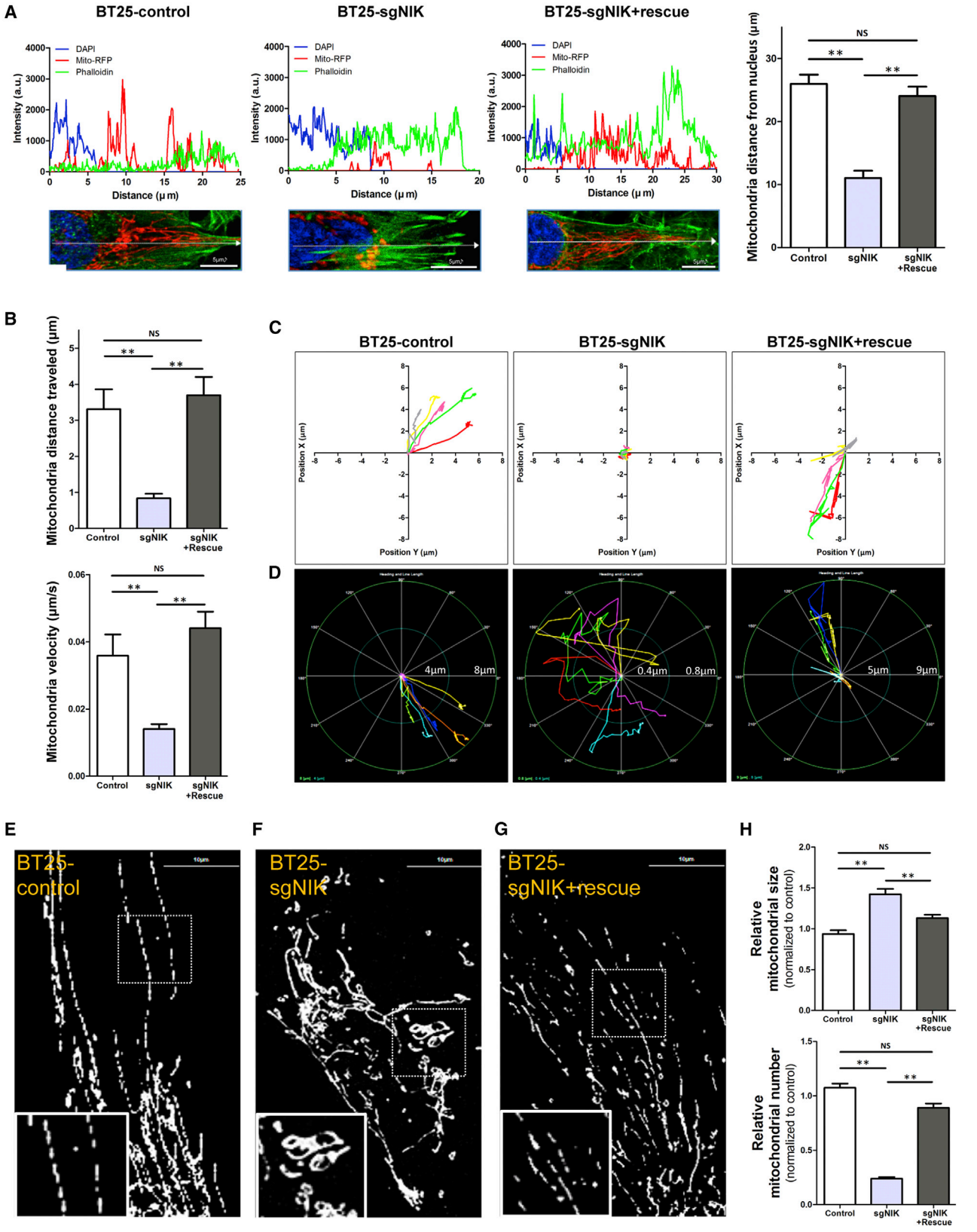

(legend on next page)

(Figure 3F), a phenotype that was reversed by murine NIK (mNIK) overexpression (Figure 3G). Particle analysis of Mito-RFP staining using ImageJ software revealed that, whereas the number of mitochondria was significantly decreased in cells lacking NIK (BT25-sgNIK cells) compared to corresponding control cells, mitochondrial size increased (Figure 3H). Conversely, NIK overexpression (BT114-hNIK cells) was associated with increased number and decreased size of mitochondria (Figure S2A).

Last, to determine whether the increased mitochondrial size in BT25-sgNIK cells reflected altered mitochondrial dynamics, we examined mitochondrial fusion in live cells using a mitochondrial matrix-targeted photoactivatable green fluorescent protein (mito-PAGFP)-based assay [24]. Fluorescence intensity in specific regions of interest had very similar rates of dissipation in BT25 control and BT25-sgNIK cells (Figures S2B and S2C), demonstrating that mitochondrial fusion is not significantly impaired in the absence of NIK. These results strongly suggested a role for NIK in promoting mitochondrial fission and trafficking.

NIK Recruits Drp1 to Mitochondria and Regulates Drp1 Phosphorylation

The GTPase dynamin-related protein 1 (Drp1) is a cytosolic factor that is recruited to mitochondria, where it promotes mitochondrial fission [25]. Accordingly, we observed punctate Drp1 immunostaining in the cytosol with some Mito-RFP co-localization (Figure 4A). No Drp1 staining was observed in BT25 cells expressing sgRNAs for CRISPR-Cas9-mediated knockout of Drp1 (BT25-sgDrp1 cells; Figures S3A and S3B), verifying antibody specificity. Intriguingly, Drp1 association with Mito-RFP was significantly diminished in BT25-sgNIK cells but was restored in BT25-sgNIK+rescue cells (Figures 4B–4D). A second Drp1 antibody, whose specificity was also verified, primarily recognized mitochondrial but not cytosolic Drp1, and also showed loss of Drp1 mitochondrial co-localization in BT25-sgNIK cells (Figure S3C).

Biochemical fractionation and immunoblot analyses confirmed that Drp1 was present in both cytosolic and mitochondria-enriched fractions of BT25 control cells (Figure 4E). In contrast, BT25-sgNIK cells exhibited diminished Drp1 protein levels specifically in the mitochondria-enriched fraction (Figure 4E). Again, mitochondrial Drp1 expression was restored in BT25-sgNIK+rescue cells (Figure 4E), demonstrating that the observed effects in BT25-sgNIK cells are mediated by NIK. The expression of other mitochondrial proteins, including mitochondrial fission factor (Mff), mitochondrial fission protein 1 (Fis1), optic atrophy 1 (Opa1), and mitofusin-1/2 (Mfn1/2), was not significantly altered in BT25-sgNIK or BT114-NIK cells compared with their respective controls (Figure S4). Similarly, Tom20 levels were not affected in mitochondrial fractions of BT25-sgNIK cells (Figure 4E), suggesting that mitochondrial membrane protein topology is not grossly altered and that NIK specifically regulates Drp1 mitochondrial localization.

Drp1 is regulated by post-translational modification, including phosphorylation at serine 616 (Drp1-P616), which is associated with enhanced mitochondrial fission, and serine 637 (Drp1-P637), which is associated with loss of fission [26, 27]. Compared to BT25 control cells, BT25-sgNIK cells exhibited decreased Drp1-P616 levels, with a concomitant increase in Drp1-P637 (Figures 4F and 4G), suggesting that NIK enhances the fission-promoting activity of Drp1. Similar to cells lacking Drp1, loss of NIK also exhibited differences in other mitochondrial functions, including a decrease in production of reactive oxygen species (ROS) and oxygen consumption (Figure S5). These results indicate that NIK regulates Drp1 mitochondrial recruitment and phosphorylation to promote mitochondrial fission.

Drp1 Interacts with NIK, but Not IKKα

To examine the subcellular distribution of NIK and Drp1, we performed co-immunostaining experiments in BT25 glioma cells. Drp1 immunoreactivity co-localized with that of NIK (Figures 5A and 5C) but did not significantly overlap with IKKα, the primary direct downstream target of NIK (Figures 5B and 5C). Similarly, we observed that NIK, but not IKKα, co-localized with Drp1 in patient-derived, ex vivo glioma tissue (Figures 5D and 5E). These data show that mitochondrial localization of NIK is an intrinsic property of primary human cancer cells, and not simply a phenotype observed in cancer cell lines in vitro. To determine whether the co-localization of Drp1 and NIK immunostaining reflected a direct interaction, we performed immunoprecipitation experiments in BT114 control and BT114-NIK-overexpressing cells. Results from these experiments indeed demonstrated that Drp1 exists in a complex with NIK but not IKKα (Figure 5F).

NIK Requires Drp1 to Promote TWEAK-Induced Invasion

We have previously demonstrated that low, endogenous concentrations of the tumor-inducing cytokine TWEAK (10 ng/mL) induce NIK expression and promote NIK-dependent invasion [4, 5]. Indeed, TWEAK treatment increases invasion of BT25 control cells to a similar extent as BT25 cells overexpressing NIK, whose invasive potential is also further potentiated by TWEAK

Figure 3. NIK Regulates Mitochondrial Morphology

(A) Fluorescence intensity profile plot of BT25 control, BT25-sgNIK, and BT25-sgNIK+rescue cells. Graphs show the immunofluorescence intensity, expressed in arbitrary units (a.u.), of Mito-RFP (red), DAPI (blue), and phalloidin (green) along the line arrows in the lower images. Scale bars, 5 μm. Right: the bar graph shows the quantification of the distance from the nucleus to mitochondria. Data are represented as mean ± SD ($n > 10$). $^{**}p < 0.01$ for sgNIK versus control and sgNIK versus sgNIK+rescue, one-way ANOVA.

(B) Plot of the run length of mobile mitochondria and velocity in cells expressing Mito-RFP as in Movie S1. Data are represented as mean ± SD of randomly selected mitochondria shown in different colors ($n > 10$ cells, respectively). $^{**}p < 0.01$.

(C and D) Vector paths of single mitochondria observed during live-cell imaging representing the tracks (C) and direction (D) of mitochondrial movement. The intersection point of the x and y axes is the starting point of each mitochondrion.

(E–G) Superresolution structured illumination microscopy was performed with the following cells expressing Mito-RFP: BT25 control (E), BT25-sgNIK (F), and (G) BT25-sgNIK+rescue (G). Images marked with white squares are magnified and shown as insets. Scale bars, 10 μm.

(H) Mitochondrial number and size in BT25 control, BT25-sgNIK, and BT25-sgNIK+rescue cells were quantified using the Analyze Particles function in ImageJ software. Data are represented as mean ± SD. $^{**}p < 0.01$ for sgNIK versus control and sgNIK versus sgNIK+rescue, one-way ANOVA ($n > 100$, respectively). See also Figure S2.

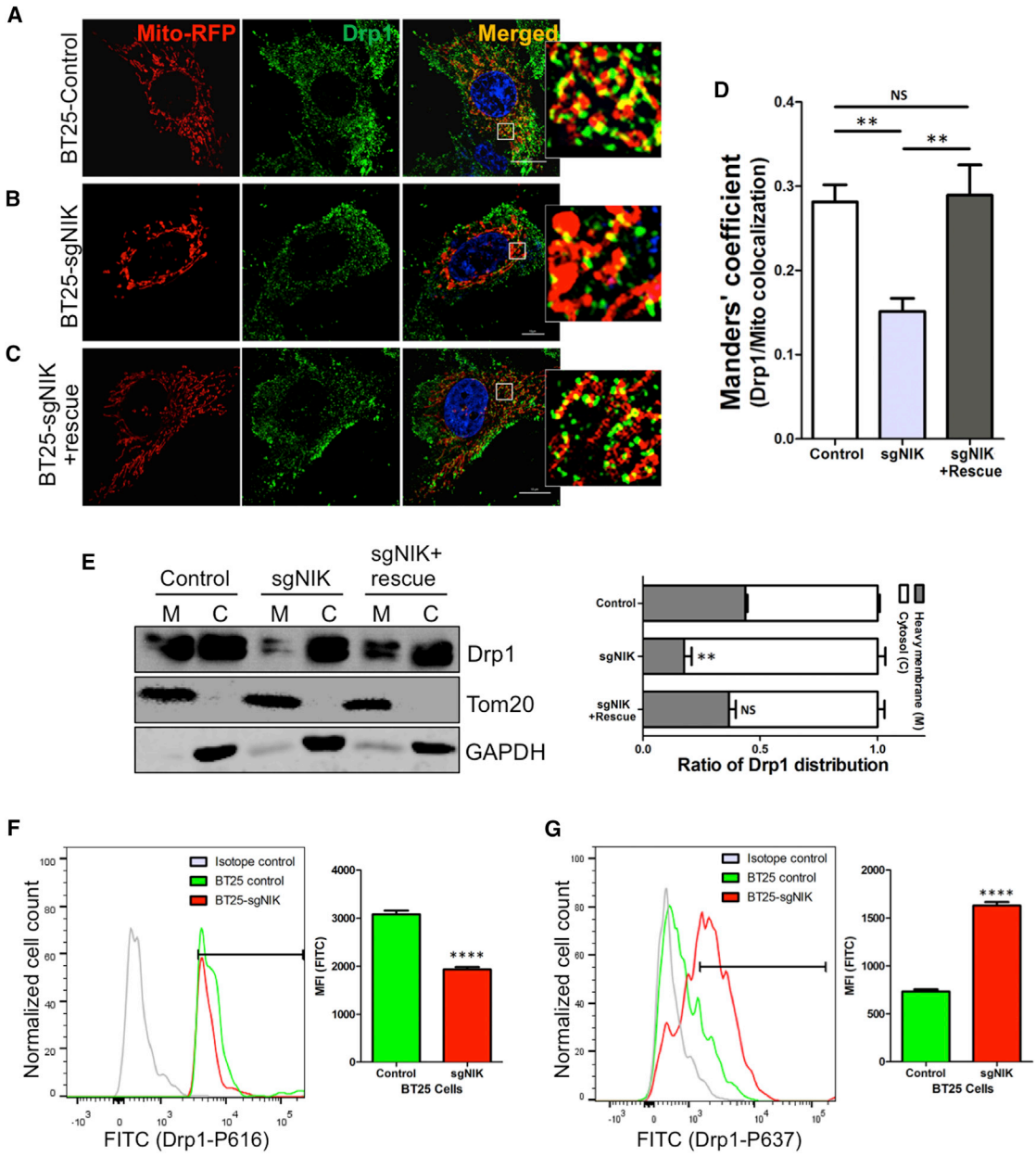

Figure 4. NIK Regulates Drp1 Recruitment to Mitochondria

(A–C) BT25 control (A), BT25-sgNIK (B), and sgNIK+rescue cells (C) were transfected with Mito-RFP to visualize mitochondria (red) and then immunostained for Drp1 (green) and DAPI (blue). Areas within the white squares are amplified and shown on the right. Scale bars, 10 μm.

(D) Bar graph showing Manders' coefficients for co-localization of Drp1 and Mito-RFP (A–C). Data are represented as mean ± SD (n > 8). **p < 0.01 for sgNIK versus control and sgNIK versus sgNIK+rescue, one-way ANOVA.

(E) Immunoblot analysis of mitochondria-enriched (M) and cytosolic (C) fractions prepared from BT25 control, BT25-sgNIK, and BT25-sgNIK+rescue cells was performed with the indicated antibodies. Results are representative of five separate experiments. Right: the bar graph shows quantification of the ratio of Drp1 in cytosolic and mitochondria-enriched heavy membrane fractions. Data are represented as mean ± SD. **p < 0.01 for sgNIK versus control and sgNIK versus sgNIK+rescue, one-way ANOVA.

(F and G) Flow cytometric histogram measuring levels of Drp1-PS616 (F) and Drp1-PS637 (G) in BT25 control (green) and sgNIK cells (red). Isotype control is shown in gray. Right: the bar graphs show mean fluorescence intensity (MFI) values for control and sgNIK cells. Data are represented as mean ± SEM. ****p < 0.0001, unpaired t test.

See also Figures S3–S5.

(Figure 6A). As expected, loss of NIK (sgNIK) almost completely abrogates both basal and TWEAK-induced invasion [5], and this invasion defect was completely rescued by NIK overexpression (sgNIK+NIK) (Figure 6A). To assess whether NIK acts through Drp1, we measured invasion of TWEAK-treated BT25-sgDrp1 cells. Indeed, these cells displayed strongly attenuated invasion,

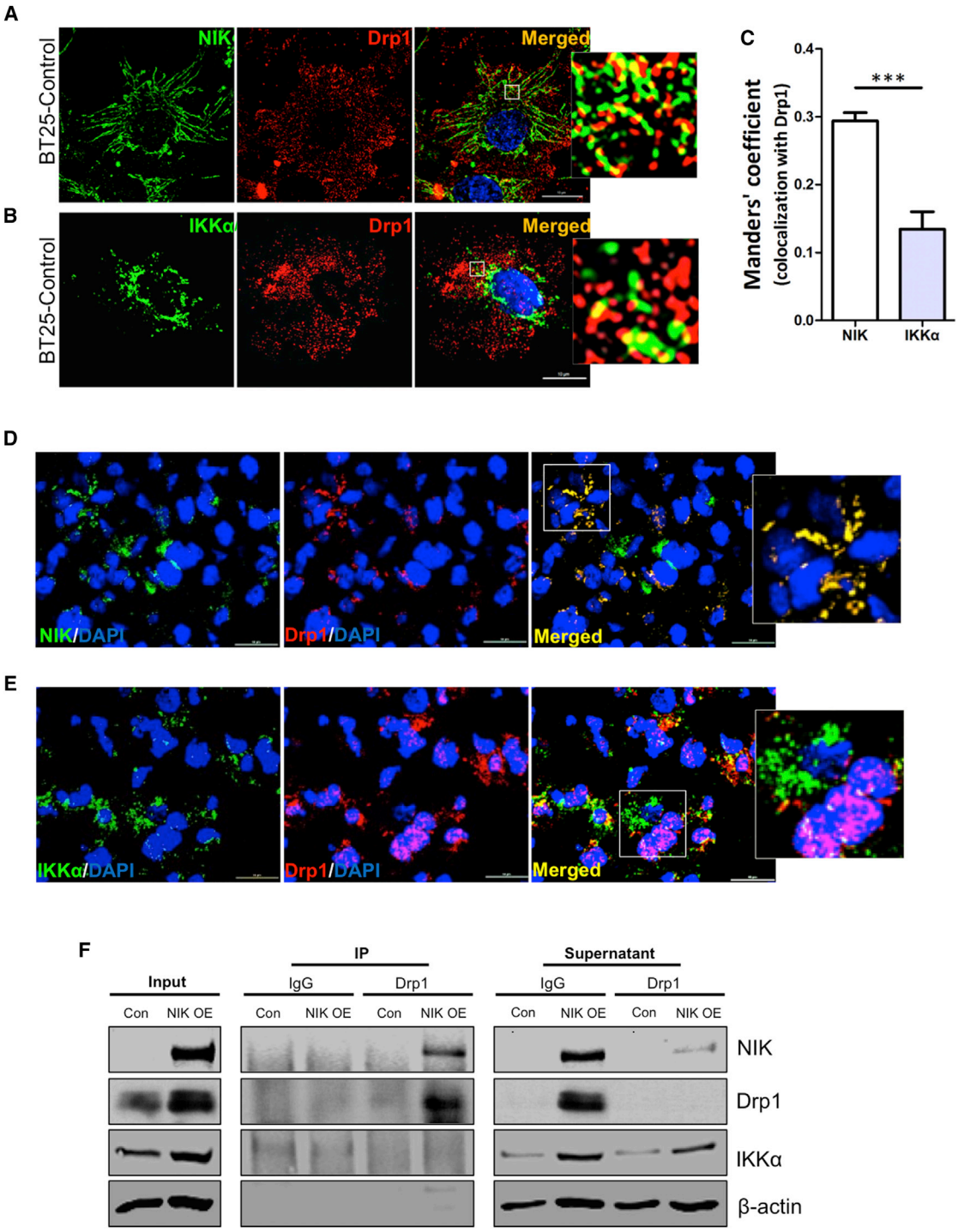

Figure 5. Drp1 Interacts with NIK but Not IKKα

(A) BT25 control cells were immunostained for NIK (green), Drp1 (red), and DAPI (blue). The image marked with a white square is amplified and shown on the right. Scale bar, 10 μm.

(B) BT25 control cells were immunostained for IKKα (green), Drp1 (red), and DAPI (blue). The image marked with a white square is amplified and shown on the right. Scale bar, 10 μm.

(C) Bar graph showing Manders' coefficients for co-localization of Drp1 and NIK or IKKα (A and B). Data are represented as mean ± SEM (n = 9). ***$p < 0.001$, unpaired t test.

(D) Human glioma patient tumor sections were stained for NIK (green), Drp1 (red), and DAPI (blue). Representative images from one of four patient samples are shown. The image marked with a white square is amplified and shown on the right. Scale bars, 10 μm.

(legend continued on next page)

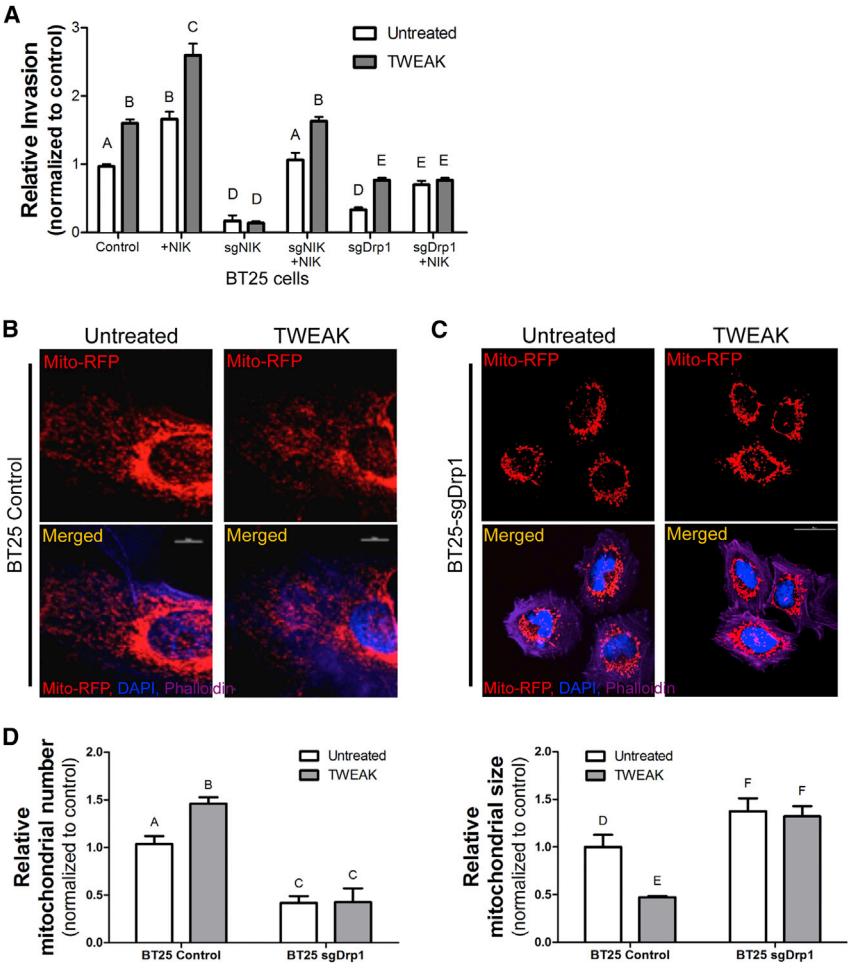

Figure 6. NIK Requires Drp1 to Promote TWEAK-Induced Invasion

(A) Quantification of 3D collagen invasion assays. The indicated cells were allowed to invade 3D collagen matrices in the absence or presence of TWEAK (10 ng/mL). Data are represented as mean ± SD (n = 3). Different letters represent statistically significant differences (for A versus B, $p < 0.001$; for A/B versus D, A versus B, and C versus E, $p < 0.0001$; for D versus E, $p < 0.05$; two-way ANOVA).

(B and C) Representative immunofluorescence images of BT25 control (B) and BT25-sgDrp1 cells (C) in the absence or presence of TWEAK (10 ng/mL) transfected with Mito-RFP (red) and stained with DAPI (blue) and phalloidin (purple). Scale bars, 10 μm.

(D) Mitochondrial number and size in BT25 control and BT25-sgDrp1 cells were quantified using the Analyze Particles function in ImageJ software. Data are represented as mean ± SD (n = 14). Different letters represent statistically significant differences (for D versus F, $p < 0.05$; for A versus B and D versus E, $p < 0.01$; for A/B versus C and E versus F, $p < 0.001$; one-way ANOVA).

similar to BT25-sgNIK cells (Figure 6A). TWEAK was still able to increase invasion in BT25-sgDrp1 cells, but to significantly lower levels than BT25 control (Figure 6A). More importantly, unlike control and BT25-sgNIK cells, NIK overexpression in BT25-sgDrp1 cells had no effect on TWEAK-induced invasion (Figure 6A). Visualization and quantification of Mito-RFP-labeled mitochondria revealed that whereas TWEAK increased the number of small, punctate mitochondria in BT25 control cells (Figures 6B and 6D), it had no effect on BT25-sgDrp1 cells, which also exhibited collapsed, fused mitochondria, similar to BT25-sgNIK cells (Figures 6C and 6D). These results suggest that Drp1 activity and mitochondrial fission are important downstream mediators of NIK-dependent, TWEAK-induced cancer cell invasion.

NIK Enhances the Invasive Potential of Mouse Embryonic Fibroblasts in the Absence of IKK/NF-κB Signaling

Lack of significant co-localization or interaction between IKKα and Drp1 in glioma cells (Figures 5B, 5E, and 5F) led us to investigate whether NIK regulates invasion and mitochondrial functions independent of IKK. We took advantage of mouse embryonic fibroblasts (MEFs), which are able to invade 3D collagen matrices, similar to glioma cells [5, 28]. Additionally, MEFs derived from IKKα/β null mice [29] (referred to as ΔIKK MEFs) provide a genetic tool to assess NIK function in the absence of IKK and downstream NF-κB signaling. Immunofluorescence experiments in MEFs revealed that NIK broadly co-localized with Mito-RFP and Tom20 (Figure 7A; Figure S6A) and had minimal overlap with the ER protein Sec61 (Figure S6B), similar to glioma cells. As expected, MEFs in which NIK was knocked out using sgRNA-mediated CRISPR-Cas9 genome editing (sgNIK MEFs) lacked any NIK protein, both by immunostaining and immunoblot analyses (Figures 7A and 7B). NIK was observed in mitochondria-enriched MEF cell fractions (Figure 7B), and did not co-localize with IKKα (Figures S6C and S6D).

Compared to WT MEFs, sgNIK MEFs exhibited substantially diminished invasion in collagen, and overexpression of human NIK increased invasion (Figures S7A and S7B). ΔIKK MEFs were somewhat less invasive compared to WT (Figure 7C). Similar to WT, deletion of NIK in ΔIKK MEFs (sgNIK-ΔIKK MEFs) further attenuated invasion (Figure 7D), whereas overexpression of hNIK (ΔIKK MEFs+hNIK) increased invasion (Figure 7E). Importantly, hNIK overexpression in ΔIKK MEFs did not activate downstream NF-κB signaling, assessed by the lack of any increased p100 processing to p52, p65 (S536)

(E) Adjacent tumor sections from (D) were stained with IKKα (green), Drp1 (red), and DAPI (blue). The image marked with a white square is amplified and shown on the right. Scale bars, 10 μm.

(F) BT114 control and BT114-hNIK cell lysates were subjected to immunoprecipitation (IP) with control immunoglobulin G (IgG) or a Drp1 antibody against endogenous Drp1. The immunoprecipitates were analyzed by immunoblotting with the indicated antibodies.

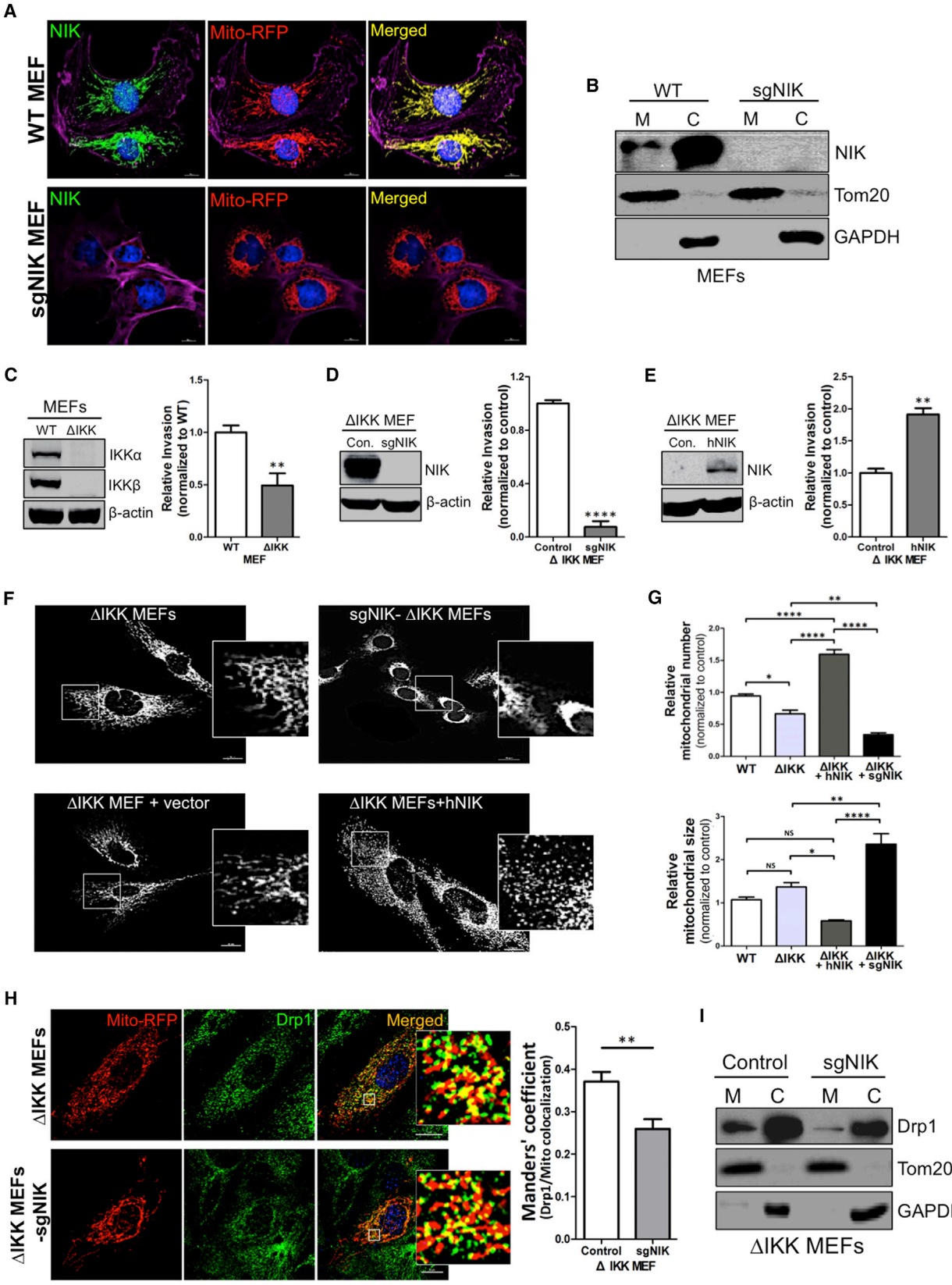

(legend on next page)

phosphorylation, or nuclear accumulation of p65, RelB, or p52 (Figure S7C). Furthermore, unlike WT MEFs, ΔIKK MEFs overexpressing NIK did not exhibit increased expression of the NF-κB target gene MMP9 (Figures S7D and S7E) [30–32]. These data clearly show that the NIK-dependent invasive potential of MEFs is uncoupled from IKK/NF-κB signaling.

Finally, loss of NIK in WT and ΔIKK MEFs resulted in collapsed, perinuclear Mito-RFP staining (Figure 7F; Figure S7F), similar to BT25-sgNIK, Panc1-sgNIK, and MDA-MB231-sgNIK cells (Figure 1D; Figures S1C and S1D). Moreover, overexpression of NIK in both WT and ΔIKK MEFs increased the appearance of punctate mitochondria dispersed throughout the cytoplasm (Figure 7F; Figure S7G). Particle analysis of Mito-RFP staining revealed that although the number of mitochondria was significantly decreased in ΔIKK MEFs compared to corresponding WT MEFs, mitochondrial size was increased (Figure 7G). Conversely, NIK overexpression in ΔIKK MEFs (ΔIKK+hNIK) was associated with increased number and decreased size of mitochondria (Figure 7G). Similar to BT25 cells, ΔIKK MEFs also exhibited co-localization of Drp1 with Mito-RFP, which was significantly diminished in sgNIK-ΔIKK MEFs (Figure 7H). Biochemical fractionation and immunoblot analyses confirmed loss of Drp1 protein specifically in the mitochondria-enriched fraction of sgNIK-ΔIKK MEFs (Figure 7I). Taken together, these data demonstrate that NIK regulates Drp1 mitochondrial localization and promotes cell invasion independent of IKK/NF-κB.

DISCUSSION

The present study establishes several novel features of NIK in cancer cells. We identify a previously unrecognized pool of NIK protein in mitochondria. Moreover, we demonstrate that NIK regulates the phosphorylation and subcellular localization of the master fission protein Drp1 to control mitochondrial dynamics, velocity, and directional migration to the periphery of migrating cells. We find that NIK regulation of mitochondrial functions and cell invasion does not require the known NIK targets IKKα and IKKβ, and hence is very likely independent of NF-κB signaling.

Based on biochemical cell-fractionation and immunofluorescence staining experiments, we propose that NIK exists in at least two protein pools: a proteasome-associated cytosolic pool primarily mediating IKK/NF-κB signaling, and a mitochondrial pool regulating Drp1 recruitment and mitochondrial dynamics (Figure 7). The discovery of a discrete mitochondria-associated fraction of NIK was unexpected, given that NIK has been described primarily as a cytosolic protein that is constitutively degraded in the absence of stimuli [15]. Indeed, this property renders endogenous NIK difficult to detect by immunoblotting under basal conditions and in the absence of proteasome inhibition (see Figure 1M and Figure S7B). Regardless, distinct NIK immunostaining is observed in mitochondria under unstimulated conditions in different cancer cell lines and immortalized MEFs. NIK mitochondrial localization was observed in MEFs and all cancer cells examined using two different antibodies (see Figure 2), and their specificity was verified by loss of signal in NIK knockout cells. Most importantly, both the mitochondrial defects and NIK mitochondrial localization in NIK knockout cells were rescued by expression of mNIK. We surmise that the discrepancy between immunoblot analysis, which detects both cytosolic and mitochondrial NIK, and immunofluorescence, which detects only mitochondrial NIK, may be due to differences in the ability of the antibodies to interact with the NIK epitope in its native conformation in different cellular compartments. For example, factors present in the cytosol, but absent in mitochondria, might associate with NIK, and either alter its conformation or sequester its epitope. In support of this interpretation, we found a Drp1-specific antibody that recognizes mitochondria-associated, but not cytosolic, Drp1 (Figure S3). Alternatively, the majority of soluble, cytosolic NIK may be lost during the immunostaining procedure, and/or NIK detection in the mitochondria by immunofluorescence may be enhanced by its oligomerization at this site. Similar to Drp1, whose oligomerization is critical for its fission-promoting activity [33], NIK is capable of

Figure 7. NIK Enhances the Invasive Potential of MEFs in the Absence of IKK/NF-κB Signaling

(A) Representative immunofluorescence confocal images of WT and NIK knockouts (sgNIK MEFs) that were transfected with Mito-RFP (red) to visualize mitochondria and then fixed and immunostained for NIK (green), DAPI (blue), and phalloidin (purple). Scale bars, 10 μm.

(B) Immunoblot analysis of mitochondria-enriched (M) and cytosolic (C) fractions prepared from WT and sgNIK MEFs pre-treated with TWEAK (10 ng/mL) and MG132 (5 μM) to stabilize NIK for facile detection and to confirm the loss of NIK in sgNIK MEFs. Blots were probed with the indicated antibodies (mitochondria-enriched/cytosol 4:1 in volume equivalents).

(C) Left: immunoblot analysis of whole-cell lysates prepared from untreated WT MEFs and ΔIKK MEFs probed with the indicated antibodies. Right: quantification of 3D collagen invasion assays comparing WT MEFs and ΔIKK MEFs. $^{**}p < 0.01$, unpaired t test.

(D) Left: immunoblot analysis of whole-cell lysates prepared from ΔIKK MEFs expressing vector (control) or NIK knockout (sgNIK-ΔIKK MEFs) probed with the indicated antibodies. Cells were pre-treated with TWEAK and MG132. Right: quantification of 3D collagen invasion assays comparing ΔIKK MEFs and sgNIK-ΔIKK MEFs; $^{****}p < 0.0001$, unpaired t test.

(E) Left: immunoblot analysis of whole-cell lysates from untreated ΔIKK MEFs expressing vector (control) or hNIK performed with the indicated antibodies. Right: quantification of 3D collagen invasion assays comparing ΔIKK MEFs expressing vector control or hNIK; $^{**}p < 0.01$, unpaired t test.

(F) Representative immunofluorescence confocal images of ΔIKK MEFs, ΔIKK MEFs+vector, sgNIK-ΔIKK MEFs, and ΔIKK MEFs+hNIK that were transfected with Mito-RFP (grayscale) to visualize mitochondria. Images marked with white squares are amplified and shown on the right. Scale bars, 10 μm.

(G) Mitochondrial number and size in WT MEFs, ΔIKK MEFs, ΔIKK MEFs+hNIK, and sgNIK-ΔIKK MEFs were quantified using the Analyze Particles function in ImageJ software. Data are represented as mean ± SD ($n > 16$). $^{*}p < 0.05$, $^{**}p < 0.01$, $^{****}p < 0.0001$, one-way ANOVA.

(H) ΔIKK MEFs and sgNIK-ΔIKK MEFs were transfected with Mito-RFP to visualize mitochondria (red) and immunostained for Drp1 (green) and DAPI (blue). Images marked with white squares are amplified and shown on the right. Scale bars, 10 μm. Right: the bar graph shows Manders' coefficients (fraction of Drp1 in co-localization with Mito-RFP) for co-localization of Drp1 and mitochondria. Data are represented as mean ± SEM ($n > 14$). $^{**}p < 0.01$, unpaired t test.

(I) Immunoblot analysis of mitochondria-enriched (M) and cytosolic (C) fractions from ΔIKK MEFs and sgNIK-ΔIKK MEFs was performed with the indicated antibodies.

See also Figures S6 and S7.

forming homotypic oligomers [34], for which a biological function has not yet been established. Although our studies have unambiguously identified a pool of NIK in mitochondria, we cannot rule out the possibility that some NIK protein may localize with other organelles, such as peroxisomes, the ER, mitochondria-associated membrane [35], or mitochondria-derived vesicles [36]. In this context, we note that a relatively small fraction of NIK was reported to co-localize with Rab5^{+} endosomes in human endothelial cells [23]. However, in cancer cells, NIK does not co-localize with Rab5 or ER markers (Figure 2). Thus, it is possible that NIK has distinct roles and subcellular localizations in different cell types.

Because NIK lacks a mitochondrial targeting sequence (MTS), it is most likely recruited to, and retained in, the mitochondria through interactions with a protein containing an MTS [37]. Potential candidates include the mitochondrial heat shock protein 90 (Hsp90), which is not only a known chaperone of NIK [38], but was also found to deliver proteins to mitochondrial import receptors [39, 40]. Alternatively, mitochondrial localization of NIK may involve localized, co-translational mitochondrial import [41], which could potentially facilitate its protection from being immediately ubiquitinated and degraded. Localization of NIK to mitochondria, its presence in a complex with Drp1, and its regulatory role in Drp1 phosphorylation and mitochondrial localization suggest that NIK functions as a novel fission "sensor." Thus, it will be interesting to determine whether the association of NIK with mitochondria is dynamic, and possibly induced by specific signals known to promote fission [26, 42–44].

Our imaging studies have identified a role for NIK in regulating the velocity and anterograde movement of mitochondria toward the periphery of migrating cells, suggesting that increased fission, mitochondrial motility, and cell invasion are functionally linked. This hypothesis is supported by the striking phenotype of diverse cancer cells and MEFs lacking NIK, which exhibit less fragmented mitochondria that are concentrated in the perinuclear region (Figures 1C, 3F, 4B, and 7F; Figure S7F). It remains to be investigated whether NIK regulates the motor proteins on the mitochondrial surface, such as kinesin and Miro [45]. Additionally, in light of recent findings demonstrating a critical role for ER-associated actin in regulating mitochondrial fission [33, 46], future studies are necessary to address whether NIK participates in establishing contacts between mitochondria and the ER at sites of fission, or in regulating calcium flux, which was recently demonstrated to be required for cancer cell migration [47].

Although we found that NIK forms a complex with Drp1, its regulation of Drp1 phosphorylation may be mediated indirectly. It was recently reported that Erk2 promotes tumorigenesis through phosphorylation of Drp1-serine 616, resulting in increased mitochondrial fission activity [48]. Thus, NIK may regulate Drp1 phosphorylation indirectly through its ability to phosphorylate Erk [49]. Additionally, the increase of Drp1-P637 observed in BT25-sgNIK cells suggests that NIK may regulate a phosphatase that dephosphorylates Drp1. Indeed, a recent study of the NIK interactome identified several mitochondrial membrane proteins, including phosphoglycerate mutase family member 5 (PGAM5), a Drp1-P637 phosphatase [50]. Alternatively, NIK may regulate Drp1 at other steps, such as oligomeric maturation [33] or GTP hydrolysis [51]. Future studies are needed to clarify these molecular mechanisms.

The recruitment of Drp1 to mitochondria is mediated by several mitochondrial outer-membrane proteins, including Mff and Fis1 [52–54]. *Mff* null and *Fis1* null cells appear interconnected yet elongated [55], whereas mitochondria in cells lacking NIK appear tangled and collapsed within the perinuclear region, similar to *Drp1* null cells (compare Figure 1D to Figure 6C). We also note the presence of circularized mitochondria in glioma cells lacking NIK (Figure 3F), which is indicative of mitochondrial damage and stress [56]. These results suggest that NIK may regulate other mitochondrial functions, and indeed we have observed that loss of NIK decreases ROS and oxygen consumption, similar to cells lacking Drp1 (Figure S5). Regardless, our data support a model in which NIK is a regulatory component of the mitochondrial fission machinery that plays a central role in cancer cell invasion.

Lastly, we propose that NIK's function in mitochondria is independent of IKK/NF-κB signaling because it supports an expansive mitochondrial network, promotes Drp1 mitochondrial recruitment, and enhances invasive potential in the absence of IKKα or IKKβ (Figure 7). To our knowledge, this is the first report of IKK-independent functions for NIK in cancer. However, our data do not exclude the possibility that other mitochondrial functions of NIK may involve regulation by the IKK/NF-κB axis, particularly in light of studies identifying other NF-κB proteins localized to mitochondria [57], NF-κB-dependent control of mitochondrial biogenesis [58, 59], IKKα-dependent regulation of the fusion protein Opa1 [60], and NIK-IKKα association with mitochondrial antiviral signaling in response to viral infection [61].

In conclusion, we have uncovered new roles for NIK in regulating mitochondrial dynamics and tumor cell invasion, highlighting the emerging importance of NIK signaling in cancer.

EXPERIMENTAL PROCEDURES

Reagents

Antibodies for immunostaining were NIK (ab191591), IKKα (ab32041), and Drp1 (ab56788) from Abcam. Antibodies for immunoblotting were IKKα (CST2682), IKK (CST2684), NIK (CST4994), Drp1 (CST8570), and Tom20 (CST42406) from Cell Signaling Technology and GAPDH (sc137179) and β-actin (sc69879) from Santa Cruz Biotechnology. Antibodies for flow cytometry were Drp-P637 (CST4867S) and Drp-P616 (CST3455S) from Cell Signaling Technology. CellLight Mitochondria-RFP, BacMam 2.0 (Mito-RFP; C10601) was from Life Technologies. MG132 (2194S) was from Cell Signaling Technology. Collagen type I (354249) was purchased from Corning. Recombinant human (rh)TWEAK (310-06) was obtained from PeproTech.

Cell Lines

BT25 and BT114 cell lines were obtained from human glioma patients as previously described [62]. These cell lines were maintained as spheroids in neural stem cell medium containing DMEM/F-12, 1× B-27 supplement minus vitamin A, 1× GlutaMAX, 25 ng/mL EGF, 25 ng/mL basic fibroblast growth factor (bFGF), and 1× penicillin/streptomycin (Life Technologies). 293T cells were obtained from ATCC. ΔIKK MEFs were a kind gift from Al Baldwin. MEFs and HEK293T cells were cultured in DMEM with 10% FBS and 1× penicillin/streptomycin. MDA-MB231 and Panc1 were from ATCC and cultured in RPMI medium with 10% FBS and 1× penicillin/streptomycin. All cells were cultured at 37°C with 95% humidity and 5% CO_2.

CRISPR-Cas9 Gene Knockout

NIK

Oligomers encoding sgRNAs for human NIK (sgNIK-1, 5′-GCUCCUUCGG AGAGGUGCAC-3′; sgNIK-2, 5′-GAAAGCGUCGCAGCAAAGCC-3′; sgNIK-3, 5′-AGUACCGAGAAGAAGUCCAC-3′) and sgRNAs for mouse NIK (sgNIK-4,

5′-AGGAUGGGGCAUUCCGCUGU-3′; sgNIK-5, 5′-UGGAGCGCAUGCACCAGGUA-3′; sgNIK-6, 5′-AGUAUCGAGAAGAGGUCCAC-3′) were cloned into lentiCRISPR v2 (Addgene). WT and ΔIKK MEFs and BT25, Panc1, and MDA-MB231 cells were transduced with a mixture of lentiviruses carrying the three mouse or human sgRNAs. Loss of NIK expression was confirmed by immunoblotting, qPCR, and/or immunofluorescence microscopy analysis of puromycin-resistant cells. BT25-sgNIK cells and sgNIK MEFs, single-colony cells were isolated by serial dilution, and experiments were repeated with at least two clones. Panc1-sgNIK and MDA-MB231-sgNIK cells were analyzed as mixed clones. For controls, cells were transduced with empty lentiCRISPR v2.

Drp1

Oligomers encoding sgRNAs for human Drp1 (sgDrp-1, 5′-GUUCCCACUACGACGAUUUG-3′; sgDrp1-2, 5′-GCUGCCUCAAAUCGUCGUAG-3′; sgDrp1-3, 5′-GUGACAAUUCCAGUACCUCU-3′) were cloned into lentiCRISPR v2. BT25 cells were transduced with a mixture of three lentiviruses carrying the human sgRNAs, selected against puromycin, and then subjected to clonal Drp1 knockout screening. Experiments were repeated with at least two clones.

Immunofluorescence Staining

Cells (2×10^4) were seeded on eight-well chamber slides (Ibidi; 80827) or on coverslips in the presence of 0.5% FBS and allowed to adhere for 4 hr. Cells were transfected with Mito-RFP (for mitochondrial labeling; Invitrogen; C10508) for 16 hr, fixed with 4% paraformaldehyde, permeabilized for 20 min with 0.3% Triton X-100 in PBS, and blocked for 30 min at room temperature with 5% serum corresponding to the secondary antibody host. Cells were incubated overnight in 0.1% Triton X-100, 1% BSA in PBS at 4°C with primary antibody. Cells were then incubated in 1% BSA for 1 hr at room temperature with secondary antibody Alexa Fluor 488 (A11008) or Alexa Fluor 594 (A11005) from Life Technologies. Dual and triple immunostaining were performed sequentially; cells were incubated with the first primary antibody in 1% BSA overnight at 4°C, washed with PBS, and incubated with the corresponding secondary antibody in 1% BSA for 1 hr at room temperature in the dark. After washing with PBS, cells were blocked for a second time with the corresponding host serum (5%) for 30 min at room temperature, and incubated with the second primary antibody from a different species followed by the appropriate secondary antibody. For immunostaining with two rabbit antibodies (see Figure 2A), commercially pre-labeled antibodies or custom-labeled antibodies generated with an antibody labeling kit (Invitrogen; A20181) were used, and the pre-labeled antibody was used last. Cells were counterstained with the nuclear stain DAPI (Invitrogen; P36931) and phalloidin (Invitrogen; A22287) as indicated.

Human Glioma Ex Vivo Tissue Staining

The use of de-identified human glioblastoma tissue samples was approved by the Institutional Review Boards (IRBs) of both St. Joseph Regional Health Center (IRB2012-001) and Texas A&M University (IRB2014-0318D). Ex vivo tissue was immediately snap frozen in OCT on dry ice. Sections of human glioma biopsy samples were fixed with 4% paraformaldehyde and immunostained with antibodies specific for NIK, IKKα, and Drp1 (see Immunofluorescence Staining above).

Image Acquisition

Images were acquired with a Nikon TI A1R inverted confocal microscope with a CFI60 Plan Apochromat Lambda 60× oil-immersion objective lens. The Zeiss ELYRA S.1 superresolution microscope with a Plan Apochromat 63× objective/1.4 NA oil objective was used for superresolution microscopy. Images were acquired with the following scan parameters: a "frame" scan mode of 1,024 × 1,024 pixels with a 16-bit depth and a grating of three rotations. For imaging the mitochondria, 561-nm excitation was used and emission was collected with a BP 570- to 620-nm filter. Fluorescence intensity was collected using an sCMOS pco.edge electron multiplying charge coupled device (EMCCD) camera with exposure time set to 100 ms.

Quantification of Mitochondrial Number, Size, and Motility

All Mito-RFP images were taken on a Nikon TI A1R inverted confocal microscope or Nikon Eclipse Ti microscope with similar contrast and at the same magnification. Each particle in individual cells was outlined and measured for mitochondrial number and average size utilizing the Analyze Particles function in ImageJ (NIH) [63]. BT25 cells were plated on eight-well chamber slides with a glass bottom and incubated with CellLight Mitochondria-RFP BacMam reagent (C10601). After 18 hr, time-lapse imaging was performed every 10 s for 5 min, and movies of mitochondria were acquired at a rate of 5.2 frames per s using a Nikon TI A1R inverted confocal microscope with 60× Plan Apochromat lenses and stage-top incubator system. NIS Elements software (Nikon) with tracking module was used to track and analyze the movement of single mitochondria.

Additional experimental procedures can be found in the Supplemental Information.

SUPPLEMENTAL INFORMATION

Supplemental Information includes Supplemental Experimental Procedures, seven figures, and five movies and can be found with this article online at http://dx.doi.org/10.1016/j.cub.2016.10.009.

AUTHOR CONTRIBUTIONS

Conceptualization, R.S.; Methodology, R.S., J.-U.J., and S.R.; Investigation, J.-U.J., S.R., D.W.L., K.M., and M.L.K.; Validation & Visualization, K.M. and M.L.K.; Writing – Original Draft, R.S.; Writing – Review & Editing, R.S., J.-U.J., and S.R.; Resources, L.G.T.; Funding Acquisition & Project Administration, R.S.

ACKNOWLEDGMENTS

We thank Drs. Roula Mouneimne and Bob Burghardt from the TAMU Cell Imaging Facility for assistance with superresolution microscopy, and Dr. Robert Alaniz and Jane Miller in the TAMHSC College of Medicine Cell Analysis Facility for data acquisition and support with flow cytometry. ΔIKK MEFs were generously provided by Dr. Al Baldwin (UNC Chapel Hill). We also thank Drs. Hubert Amrein, Vytas Bankaitis, and Sally Ward (TAMHSC) for critical reading of the manuscript, and Dr. David Chan (Cal Tech) for helpful discussion. This work was funded by grants from the NIH (R01NS082554 to R.S.), Cancer Prevention and Research Institute of Texas HIHR award (RP160842 to R.S.), and The Texas Brain and Spine Institute (2016 seed grant to L.G.T. and R.S.).

Received: April 29, 2016
Revised: August 15, 2016
Accepted: October 4, 2016
Published: November 23, 2016

REFERENCES

1. Thu, Y.M., and Richmond, A. (2010). NF-κB inducing kinase: a key regulator in the immune system and in cancer. Cytokine Growth Factor Rev. *21*, 213–226.
2. Xia, Y., Shen, S., and Verma, I.M. (2014). NF-κB, an active player in human cancers. Cancer Immunol. Res. *2*, 823–830.
3. Lee, D.W., Ramakrishnan, D., Valenta, J., Parney, I.F., Bayless, K.J., and Sitcheran, R. (2013). The NF-κB RelB protein is an oncogenic driver of mesenchymal glioma. PLoS ONE *8*, e57489.
4. Cherry, E.M., Lee, D.W., Jung, J.-U., and Sitcheran, R. (2015). Tumor necrosis factor-like weak inducer of apoptosis (TWEAK) promotes glioma cell invasion through induction of NF-κB-inducing kinase (NIK) and noncanonical NF-κB signaling. Mol. Cancer *14*, 9.
5. Duran, C.L., Lee, D.W., Jung, J.U., Ravi, S., Pogue, C.B., Toussaint, L.G., Bayless, K.J., and Sitcheran, R. (2016). NIK regulates MT1-MMP activity and promotes glioma cell invasion independently of the canonical NF-κB pathway. Oncogenesis *5*, e231.
6. Murphy, D.A., and Courtneidge, S.A. (2011). The 'ins' and 'outs' of podosomes and invadopodia: characteristics, formation and function. Nat. Rev. Mol. Cell Biol. *12*, 413–426.
7. Arismendi-Morillo, G., Hoa, N.T., Ge, L., and Jadus, M.R. (2012). Mitochondrial network in glioma's invadopodia displays an activated state

both in situ and in vitro: potential functional implications. Ultrastruct. Pathol. *36*, 409–414.

8. Desai, S.P., Bhatia, S.N., Toner, M., and Irimia, D. (2013). Mitochondrial localization and the persistent migration of epithelial cancer cells. Biophys. J. *104*, 2077–2088.
9. Ferreira-da-Silva, A., Valacca, C., Rios, E., Pópulo, H., Soares, P., Sobrinho-Simões, M., Scorrano, L., Máximo, V., and Campello, S. (2015). Mitochondrial dynamics protein Drp1 is overexpressed in oncocytic thyroid tumors and regulates cancer cell migration. PLoS ONE *10*, e0122308.
10. Zhao, J., Zhang, J., Yu, M., Xie, Y., Huang, Y., Wolff, D.W., Abel, P.W., and Tu, Y. (2013). Mitochondrial dynamics regulates migration and invasion of breast cancer cells. Oncogene *32*, 4814–4824.
11. Caino, M.C., and Altieri, D.C. (2015). Cancer cells exploit adaptive mitochondrial dynamics to increase tumor cell invasion. Cell Cycle *14*, 3242–3247.
12. Arismendi-Morillo, G. (2009). Electron microscopy morphology of the mitochondrial network in human cancer. Int. J. Biochem. Cell Biol. *41*, 2062–2068.
13. Senft, D., and Ronai, Z.A. (2016). Regulators of mitochondrial dynamics in cancer. Curr. Opin. Cell Biol. *39*, 43–52.
14. Liu, J., Sudom, A., Min, X., Cao, Z., Gao, X., Ayres, M., Lee, F., Cao, P., Johnstone, S., Plotnikova, O., et al. (2012). Structure of the nuclear factor κB-inducing kinase (NIK) kinase domain reveals a constitutively active conformation. J. Biol. Chem. *287*, 27326–27334.
15. Sun, S.-C. (2012). The noncanonical NF-κB pathway. Immunol. Rev. *246*, 125–140.
16. Sun, S.-C. (2010). Controlling the fate of NIK: a central stage in noncanonical NF-kappaB signaling. Sci. Signal. *3*, pe18.
17. Razani, B., Reichardt, A.D., and Cheng, G. (2011). Non-canonical NF-κB signaling activation and regulation: principles and perspectives. Immunol. Rev. *244*, 44–54.
18. Oeckinghaus, A., Hayden, M.S., and Ghosh, S. (2011). Crosstalk in NF-κB signaling pathways. Nat. Immunol. *12*, 695–708.
19. Odqvist, L., Sánchez-Beato, M., Montes-Moreno, S., Martín-Sánchez, E., Pajares, R., Sánchez-Verde, L., Ortiz-Romero, P.L., Rodriguez, J., Rodríguez-Pinilla, S.M., Iniesta-Martínez, F., et al. (2013). NIK controls classical and alternative NF-κB activation and is necessary for the survival of human T-cell lymphoma cells. Clin. Cancer Res. *19*, 2319–2330.
20. Ramakrishnan, P., Wang, W., and Wallach, D. (2004). Receptor-specific signaling for both the alternative and the canonical NF-kappaB activation pathways by NF-kappaB-inducing kinase. Immunity *21*, 477–489.
21. Attanasio, F., Caldieri, G., Giacchetti, G., van Horssen, R., Wieringa, B., and Buccione, R. (2011). Novel invadopodia components revealed by differential proteomic analysis. Eur. J. Cell Biol. *90*, 115–127.
22. Dolman, N.J., Kilgore, J.A., and Davidson, M.W. (2013). A review of reagents for fluorescence microscopy of cellular compartments and structures, part I: BacMam labeling and reagents for vesicular structures. Curr. Protoc. Cytom. *65*, 12.30.1–12.30.27.
23. Jane-wit, D., Surovtseva, Y.V., Qin, L., Li, G., Liu, R., Clark, P., Manes, T.D., Wang, C., Kashgarian, M., Kirkiles-Smith, N.C., et al. (2015). Complement membrane attack complexes activate noncanonical NF-κB by forming an Akt^+ NIK^+ signalosome on $Rab5^+$ endosomes. Proc. Natl. Acad. Sci. USA *112*, 9686–9691.
24. Karbowski, M., Cleland, M.M., and Roelofs, B.A. (2014). Photoactivatable green fluorescent protein-based visualization and quantification of mitochondrial fusion and mitochondrial network complexity in living cells. Methods Enzymol. *547*, 57–73.
25. Smirnova, E., Griparic, L., Shurland, D.L., and van der Bliek, A.M. (2001). Dynamin-related protein Drp1 is required for mitochondrial division in mammalian cells. Mol. Biol. Cell *12*, 2245–2256.
26. Taguchi, N., Ishihara, N., Jofuku, A., Oka, T., and Mihara, K. (2007). Mitotic phosphorylation of dynamin-related GTPase Drp1 participates in mitochondrial fission. J. Biol. Chem. *282*, 11521–11529.
27. Chang, C.R., and Blackstone, C. (2007). Cyclic AMP-dependent protein kinase phosphorylation of Drp1 regulates its GTPase activity and mitochondrial morphology. J. Biol. Chem. *282*, 21583–21587.
28. Mierke, C.T., Kollmannsberger, P., Zitterbart, D.P., Diez, G., Koch, T.M., Marg, S., Ziegler, W.H., Goldmann, W.H., and Fabry, B. (2010). Vinculin facilitates cell invasion into three-dimensional collagen matrices. J. Biol. Chem. *285*, 13121–13130.
29. Li, Q., Estepa, G., Memet, S., Israël, A., and Verma, I.M. (2000). Complete lack of NF-kappaB activity in IKK1 and IKK2 double-deficient mice: additional defect in neurulation. Genes Dev. *14*, 1729–1733.
30. Li, H., Mittal, A., Paul, P.K., Kumar, M., Srivastava, D.S., Tyagi, S.C., and Kumar, A. (2009). Tumor necrosis factor-related weak inducer of apoptosis augments matrix metalloproteinase 9 (MMP-9) production in skeletal muscle through the activation of nuclear factor-kappaB-inducing kinase and p38 mitogen-activated protein kinase: a potential role of MMP-9 in myopathy. J. Biol. Chem. *284*, 4439–4450.
31. Fukuyama, R., Ng, K.P., Cicek, M., Kelleher, C., Niculaita, R., Casey, G., and Sizemore, N. (2007). Role of IKK and oscillatory NFkappaB kinetics in MMP-9 gene expression and chemoresistance to 5-fluorouracil in RKO colorectal cancer cells. Mol. Carcinog. *46*, 402–413.
32. Raychaudhuri, B., Han, Y., Lu, T., and Vogelbaum, M.A. (2007). Aberrant constitutive activation of nuclear factor kappaB in glioblastoma multiforme drives invasive phenotype. J. Neurooncol. *85*, 39–47.
33. Ji, W.-k., Hatch, A.L., Merrill, R.A., Strack, S., and Higgs, H.N. (2015). Actin filaments target the oligomeric maturation of the dynamin GTPase Drp1 to mitochondrial fission sites. eLife *4*, e11553.
34. Lin, X., Mu, Y., Cunningham, E.T., Jr., Marcu, K.B., Geleziunas, R., and Greene, W.C. (1998). Molecular determinants of NF-kappaB-inducing kinase action. Mol. Cell. Biol. *18*, 5899–5907.
35. Schrader, M., Godinho, L.F., Costello, J.L., and Islinger, M. (2015). The different facets of organelle interplay-an overview of organelle interactions. Front. Cell Dev. Biol. *3*, 56.
36. Sugiura, A., McLelland, G.-L., Fon, E.A., and McBride, H.M. (2014). A new pathway for mitochondrial quality control: mitochondrial-derived vesicles. EMBO J. *33*, 2142–2156.
37. Omura, T. (1998). Mitochondria-targeting sequence, a multi-role sorting sequence recognized at all steps of protein import into mitochondria. J. Biochem. *123*, 1010–1016.
38. Qing, G., Yan, P., Qu, Z., Liu, H., and Xiao, G. (2007). Hsp90 regulates processing of NF-kappa B2 p100 involving protection of NF-kappa B-inducing kinase (NIK) from autophagy-mediated degradation. Cell Res. *17*, 520–530.
39. Young, J.C., Hoogenraad, N.J., and Hartl, F.U. (2003). Molecular chaperones Hsp90 and Hsp70 deliver preproteins to the mitochondrial import receptor Tom70. Cell *112*, 41–50.
40. Fan, A.C.Y., Bhangoo, M.K., and Young, J.C. (2006). Hsp90 functions in the targeting and outer membrane translocation steps of Tom70-mediated mitochondrial import. J. Biol. Chem. *281*, 33313–33324.
41. Lesnik, C., Golani-Armon, A., and Arava, Y. (2015). Localized translation near the mitochondrial outer membrane: an update. RNA Biol. *12*, 801–809.
42. Frank, S., Gaume, B., Bergmann-Leitner, E.S., Leitner, W.W., Robert, E.G., Catez, F., Smith, C.L., and Youle, R.J. (2001). The role of dynamin-related protein 1, a mediator of mitochondrial fission, in apoptosis. Dev. Cell *1*, 515–525.
43. Wang, W., Wang, Y., Long, J., Wang, J., Haudek, S.B., Overbeek, P., Chang, B.H.J., Schumacker, P.T., and Danesh, F.R. (2012). Mitochondrial fission triggered by hyperglycemia is mediated by ROCK1 activation in podocytes and endothelial cells. Cell Metab. *15*, 186–200.
44. Willems, P.H.G.M., Rossignol, R., Dieteren, C.E.J., Murphy, M.P., and Koopman, W.J.H. (2015). Redox homeostasis and mitochondrial dynamics. Cell Metab. *22*, 207–218.
45. Wang, X., and Schwarz, T.L. (2009). The mechanism of Ca^{2+}-dependent regulation of kinesin-mediated mitochondrial motility. Cell *136*, 163–174.

46. Friedman, J.R., Lackner, L.L., West, M., DiBenedetto, J.R., Nunnari, J., and Voeltz, G.K. (2011). ER tubules mark sites of mitochondrial division. Science *334*, 358–362.

47. Tosatto, A., Sommaggio, R., Kummerow, C., Bentham, R.B., Blacker, T.S., Berecz, T., Duchen, M.R., Rosato, A., Bogeski, I., Szabadkai, G., et al. (2016). The mitochondrial calcium uniporter regulates breast cancer progression via HIF-1α. EMBO Mol. Med. *8*, 569–585.

48. Kashatus, J.A., Nascimento, A., Myers, L.J., Sher, A., Byrne, F.L., Hoehn, K.L., Counter, C.M., and Kashatus, D.F. (2015). Erk2 phosphorylation of Drp1 promotes mitochondrial fission and MAPK-driven tumor growth. Mol. Cell *57*, 537–551.

49. Nemoto, S., DiDonato, J.A., and Lin, A. (1998). Coordinate regulation of IkappaB kinases by mitogen-activated protein kinase kinase kinase 1 and NF-kappaB-inducing kinase. Mol. Cell. Biol. *18*, 7336–7343.

50. Willmann, K.L., Sacco, R., Martins, R., Garncarz, W., Krolo, A., Knapp, S., Bennett, K.L., and Boztuğ, K. (2016). Expanding the interactome of the noncanonical NF-κB signaling pathway. J. Proteome Res. *15*, 2900–2909.

51. Francy, C.A., Alvarez, F.J.D., Zhou, L., Ramachandran, R., and Mears, J.A. (2015). The mechanoenzymatic core of dynamin-related protein 1 comprises the minimal machinery required for membrane constriction. J. Biol. Chem. *290*, 11692–11703.

52. Otera, H., Wang, C., Cleland, M.M., Setoguchi, K., Yokota, S., Youle, R.J., and Mihara, K. (2010). Mff is an essential factor for mitochondrial recruitment of Drp1 during mitochondrial fission in mammalian cells. J. Cell Biol. *191*, 1141–1158.

53. Yamada, T., Adachi, Y., Iijima, M., and Sesaki, H. (2016). Making a division apparatus on mitochondria. Trends Biochem. Sci. *41*, 209–210.

54. Losón, O.C., Song, Z., Chen, H., and Chan, D.C. (2013). Fis1, Mff, MiD49, and MiD51 mediate Drp1 recruitment in mitochondrial fission. Mol. Biol. Cell *24*, 659–667.

55. Liu, R., and Chan, D.C. (2015). The mitochondrial fission receptor Mff selectively recruits oligomerized Drp1. Mol. Biol. Cell *26*, 4466–4477.

56. Ahmad, T., Aggarwal, K., Pattnaik, B., Mukherjee, S., Sethi, T., Tiwari, B.K., Kumar, M., Micheal, A., Mabalirajan, U., Ghosh, B., et al. (2013). Computational classification of mitochondrial shapes reflects stress and redox state. Cell Death Dis. *4*, e461.

57. Cogswell, P.C., Kashatus, D.F., Keifer, J.A., Guttridge, D.C., Reuther, J.Y., Bristow, C., Roy, S., Nicholson, D.W., and Baldwin, A.S., Jr. (2003). NF-kappa B and I kappa B alpha are found in the mitochondria. Evidence for regulation of mitochondrial gene expression by NF-kappa B. J. Biol. Chem. *278*, 2963–2968.

58. Bakkar, N., Ladner, K., Canan, B.D., Liyanarachchi, S., Bal, N.C., Pant, M., Periasamy, M., Li, Q., Janssen, P.M.L., and Guttridge, D.C. (2012). IKKα and alternative NF-κB regulate PGC-1β to promote oxidative muscle metabolism. J. Cell Biol. *196*, 497–511.

59. Zeng, R., Faccio, R., and Novack, D.V. (2015). Alternative NF-κB regulates RANKL-induced osteoclast differentiation and mitochondrial biogenesis via independent mechanisms. J. Bone Miner. Res. *30*, 2287–2299.

60. Laforge, M., Rodrigues, V., Silvestre, R., Gautier, C., Weil, R., Corti, O., and Estaquier, J. (2016). NF-κB pathway controls mitochondrial dynamics. Cell Death Differ. *23*, 89–98.

61. Liu, P., Li, K., Garofalo, R.P., and Brasier, A.R. (2008). Respiratory syncytial virus induces RelA release from cytoplasmic 100-kDa NF-kappaB2 complexes via a novel retinoic acid-inducible gene-I•NF-kappaB-inducing kinase signaling pathway. J. Biol. Chem. *283*, 23169–23178.

62. Kelly, J.J.P., Stechishin, O., Chojnacki, A., Lun, X., Sun, B., Senger, D.L., Forsyth, P., Auer, R.N., Dunn, J.F., Cairncross, J.G., et al. (2009). Proliferation of human glioblastoma stem cells occurs independently of exogenous mitogens. Stem Cells *27*, 1722–1733.

63. Dagda, R.K., Cherra, S.J., III, Kulich, S.M., Tandon, A., Park, D., and Chu, C.T. (2009). Loss of PINK1 function promotes mitophagy through effects on oxidative stress and mitochondrial fission. J. Biol. Chem. *284*, 13843–13855.